AGU PUBLICATIONS

Geophysical Research Letters

RESEARCH LETTER

10.1002/2017GL073236

Key Points:
- There is an abrupt transition band for upper ocean stratification, which agrees well with the edge of maximum sea ice extent of Antarctica
- Upper ocean stratification, dominated by salinity, modulates the ice production and preconditions the Antarctic maximum sea ice extent
- Stratification and Ekman transport strongly modulate the upper ocean heat redistribution, and the ocean's response to air-sea heat flux

Supporting Information:
- Supporting Information S1

Correspondence to:
Z. Su,
zssu@caltech.edu

Citation:
Su, Z. (2017), Preconditioning of Antarctic maximum sea ice extent by upper ocean stratification on a seasonal timescale, *Geophys. Res. Lett.*, *44*, 6307–6315, doi:10.1002/2017GL073236.

Received 28 FEB 2017
Accepted 3 JUN 2017
Accepted article online 6 JUN 2017
Published online 22 JUN 2017

Preconditioning of Antarctic maximum sea ice extent by upper ocean stratification on a seasonal timescale

Zhan Su[1]

[1]Jet Propulsion Laboratory, California Institute of Technology, Pasadena, California, USA

Abstract This study uses an observationally constrained and dynamically consistent ocean and sea ice state estimate. The author presents a remarkable agreement between the location of the edge of Antarctic maximum sea ice extent, reached in September, and the narrow transition band for the upper ocean (0–100 m depths) stratification, as early as April to June. To the south of this edge, the upper ocean has high stratification, which forbids convective fluxes to cross through; consequently, the ocean heat loss to the atmosphere is an efficient way to cool the surface ocean to the freezing point during April to September. To the north, the upper ocean has low stratification such that the ocean heat loss to the atmosphere is not efficient to cool the upper ocean. The upper ocean is instead cooled mainly through mixing with the colder inflow carried by northward Ekman transport but cannot reach the freezing point due to the nature of mixing. Therefore, upper ocean stratification, dominated by salinity here, provides an important constraint on the northward expansion of Antarctic sea ice to its maximum.

1. Introduction

Antarctic sea ice is a critical component of Earth's climate system. The evolution of its extent will both respond to and influence the state of the climate: e.g., it may modulate the meridional overturning circulation of the ocean [*Ferrari et al.*, 2014] and also interact with the circulation in response to anthropogenic greenhouse gas forcing [*Marshall et al.*, 2015]. Over a decadal timescale Antarctic sea ice extent has experienced a slight but statistically significant expansion (~18.6×10^4 km^2 per decade for 1979–2013 annual trend) [*Turner et al.*, 2015; *Comiso and Nishio*, 2008; *Fan et al.*, 2014]. This slight expansion is the residual of strong and opposing regional trends [e.g., *Holland*, 2014]. Over a seasonal timescale, Antarctic sea ice extent typically reaches its maximum in September of each year [e.g., *Turner et al.*, 2013].

Several factors have been suggested to be important for the evolution of Antarctic sea ice extent. These include Ekman transport and wind-driven upwelling in the Southern Ocean that influence the sea surface temperature and the thermodynamic production of ice [*Purich et al.*, 2016; *Armour et al.*, 2016; *Ferreira et al.*, 2015], wind-driven sea ice drift that can be modulated by the Southern Oscillation and Southern Annular Mode [*Holland and Kwok*, 2012; *Kwok et al.*, 2016; *Haumann et al.*, 2014], air-sea heat flux [*Stammerjohn et al.*, 2008; *Bitz et al.*, 2005], freshwater flux from the Antarctic Ice Sheet [*Bintanja et al.*, 2013], and connections to Atlantic warming [*Li et al.*, 2014]. These mechanisms have been shown to be potentially influential for the decadal variability of sea ice.

Some literature has discussed the effect of stratification on sea ice. For example, *Gordon* [1981] discussed the related effect on the retreat of sea ice. *Zhang* [2007] discussed the effect of stratification on the decadal variability of sea ice [see also *Goosse and Zunz*, 2014; *Bitz et al.*, 2005]. *Fenty and Heimbach* [2013] suggested that the upper ocean stratification significantly modulates the sea ice growth in the Labrador Sea. *Martinson* [1990] and *Martinson and Iannuzzi* [1998] analyzed the static stability of surface ocean layer below the sea ice. Their analytical models estimate that the water mass properties at the southern edge of the Antarctic Circumpolar Current directly influence the thermodynamic budget of sea ice.

This study quantitatively investigates the role of upper ocean stratification on the seasonal evolution of ice around Antarctica, using an observationally constrained and dynamically consistent ocean and sea ice state estimate. Upper ocean stratification is shown to be coupled with Ekman transport on redistributing heat vertically and horizontally. This controls thermodynamic sea ice production, in response to ocean heat loss to the atmosphere during fall and winter. The focus of this study is on a seasonal timescale and the thermodynamic

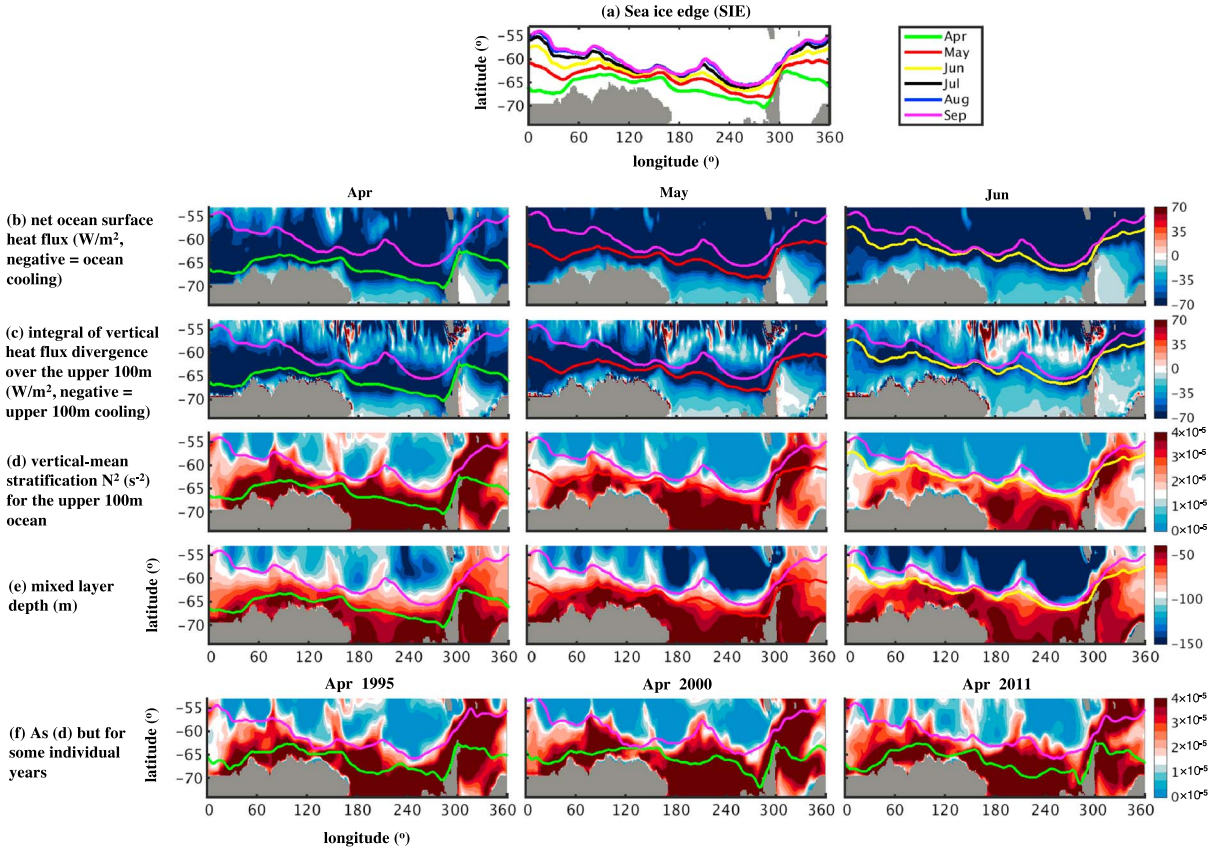

Figure 1. The results here, as well as Figures 2–3, are produced from the 1992–2015 mean monthly data of ECCO v4, except Figure 1f. (a) Sea ice edge (SIE) from April to September. The northward expansion here is most significant during April to June. (b) Net ocean surface heat flux, including air-sea and ice-sea flux, during April to June (W/m^2, negative: heat leaving the ocean). This heat flux is significant roughly to the north of the SIE for each month. (c) The integral of vertical heat flux divergence over the upper 100 m ocean (W/m^2, negative: heat leaving the upper 100 m ocean). This is equal to the vertical heat flux at the surface (Figure 1a) subtracting that at 100 m depth. The resulting cooling for upper 100 m ocean (dark blue) mainly occurs between the SIE of that month and the September SIE, as explained by Figure 1d. (d) Vertical-mean stratification for the upper 100 m ocean, represented by buoyancy frequency N^2 (s^{-2}). There is a remarkable good agreement between the location of the SIE of September (magenta curve) and the narrow band (white) for an abrupt transition of stratification (red to white to blue) during April to June. This is also generally true for individual years (see Figure 1f) and for August to September (Figure S2d). (e) Mixed layer depth (m), with further illustration in Figure 3d. (f) As Figure 1d but for the April of some random individual years.

ice production, rather than an interannual to decadal timescale and the mechanical/dynamic ice budget (i.e., wind-driven ice drift). We mainly discuss the Antarctic sea ice extent in a climatological sense, although our results also generally hold for individual years (e.g., Figure 1f versus Figure 1d, discussed later).

2. The Data Set

Even forced by realistic boundary conditions and atmospheric forcing, the state of sea ice and the upper ocean in numerical models often does not match the observations well [*Menemenlis et al.*, 2008; *Sallée et al.*, 2010]. For example, the state of sea ice and the upper ocean in a high-resolution eddy-resolving numerical model described in *Rocha et al.* [2016] deviates severely from the observations in our test. This kind of model may not be appropriate for this study, since we require realistic ice and hydrographic conditions (e.g., stratification) for an accurate description of the ice extent and its evolution. Therefore, we use an observational constrained, and also dynamically consistent, state estimate. We use the solution of ECCO v4 (Estimating the Circulation and Climate of the Ocean, version 4) [*Forget et al.*, 2015], an updated ECCO product that is found to be an acceptable fit to observations of ocean and ice (e.g., see Figure S1 in the supporting information).

The ECCO v4 solution is a recently widely used global ocean and sea ice state estimate [e.g., *Buckley and Marshall*, 2016; *Wunsch*, 2016; *Abernathey et al.*, 2016; *Liang and Yu*, 2016]. It is constrained by most available ocean and sea ice observations (e.g., satellite data and in situ profiles) of global coverage for the past two

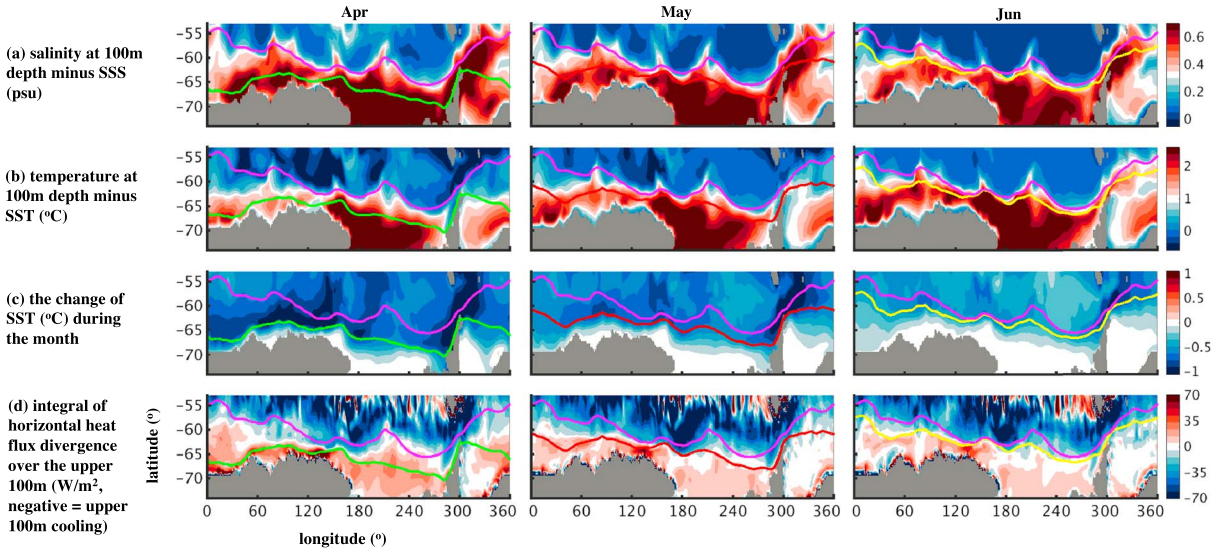

Figure 2. (a) As Figures 1b–1e but for the salinity at 100 m depth minus the sea surface salinity (SSS) (psu). (b) The temperature at 100 m depth minus the sea surface temperature (SST) (°C). From Figures 2a and 2b, the stable stratification shown in Figure 1d is caused by salinity rather than temperature. (c) The change of SST (°C) during April, May, and June, respectively. They are about the same as the change of the mean temperature of upper 100 m ocean. Here the cooling (blue) to the south and to the north of the September SIE (magenta curve) are mainly caused, respectively, by the vertical heat flux (Figure 1c) and the horizontal heat flux (Figure 2d). (d) The integral of horizontal heat flux divergence over the upper 100 m ocean (W/m^2, negative: heat leaving the upper 100 m ocean). This is mainly due to the northward Ekman transport (Figures 3a–3c, schematic in Figure 3f).

decades. More importantly, it remains dynamically consistent (i.e., fully follows the equations of motion for fluid and ice). Therefore, the mechanism for the evolution of ocean and sea ice can be diagnosed physically. ECCO v4 we use here has a nominal ~1° horizontal grid spacing and includes 50 vertical levels (detailed in *Forget et al.* [2015]). Therefore, it is not eddy resolving. The effects of mesoscale eddies, as well as convection, have been instead parameterized by subgrid-scale fluxes in ECCO v4 [*Gent and Mcwilliams*, 1990; *Gaspar et al.*, 1990]. A caveat should be noted though: submesoscale restratification has not been parameterized in ECCO v4, which may not be negligible for upper ocean process [*Fox-Kemper et al.*, 2011].

We use a recent ECCO v4 solution, which is a monthly data set over the period of 1992–2015. For this study, we mainly use the 1992–2015 mean monthly data for our climatological analysis (e.g., 1992–2015 mean data for April, May, etc.). The ECCO v4 solution shows fair agreement with satellite observations for the Antarctic maximum sea ice extent (Figure S1), represented by the sea ice edge (SIE) in September. Here the SIE is defined by a typical threshold of 15% of sea ice concentration [e.g., *Worby and Comiso*, 2004]. The difference of SIE between the ECCO v4 solution and the observations is only ~0.6° at latitude in a zonal-mean sense (Figure S1). This ~0.6° is negligibly small in contrast to the scale of the seasonal migration of SIE (~10–15° migration in latitude; Figure 1a) and essentially does not affect our analysis. This ~0.6° difference can be partly due to the difference in resolution: ~1° for ECCO v4 and ~0.25° for the observations, which may cause an uncertainty of up to ~0.75° when comparing them.

3. Vertical Heat Flux Modulated by Upper Ocean Stratification

Again, in this study, we focus on the seasonal evolution of Antarctic sea ice in a climatological sense, rather than its trend (timescale $>$ 1 year). Therefore, we use the 1992–2015 mean monthly data of ECCO v4 throughout this study, except as otherwise mentioned.

SIE expands northward from April to September (Figure 1a) across the latitudes of ~70° to ~55°S. The expansion is most significant during April to June (Figure 1a), while being much less during July to September (i.e., the respective SIEs are close to each other). Therefore, to investigate the expansion of SIE, we focus on April to June in this study. The associated conclusions for April to June, as derived from this paper, generally also hold for July to September (Figures 1 and 2 versus Figures S2 and S3). Here we investigate why the SIE expansion finally stops around the September SIE (SSIE). We investigate this from the thermodynamic point of view since our focus is on the *open-ocean* area that is preconditioned to form sea ice months later, with the

caveat that mechanical processes (sea ice drift) would certainly also influence the SIE. Note that the SIE is always an approximate contour of ~ −1.9°C sea surface temperature (SST), the freezing point of seawater at the surface. Put in another way, our question is as follows: why is the SST cooled to the freezing point *only* roughly to the south of the SSIE by preconditioning during autumn and winter? To answer this, we need to analyze the heat budget of upper ocean.

Figure 1b shows the net ocean surface heat flux (W/m^2), which includes air-sea flux and ice-sea flux, during April to June. The negative values denote heat leaving the ocean. To the south of the SIE of each month (green, red, and yellow curves for April to June, respectively), the ocean is covered by ice. The corresponding net ocean surface heat flux, especially for area where the ice concentration is close to one, is mainly the ice-sea flux and is close to zero (~white) due to the insulating effect of ice [e.g., *Martinson*, 1990]. In contrast, for large open-ocean area to the north of the SIE, the heat flux is mainly air-sea flux: there is a strong heat loss during autumn (~ −70 W/m^2 or even larger; dark blue in Figure 1b) from the ocean to the atmosphere. This is upward heat flux at sea surface. This is even true to the north of the SSIE (magenta curve, Figure 1b) and to the south of ~55°S, where there is no sea ice presence even during September. Why then is it only to the south of the SSIE that the SST can be cooled to the freezing point by air-sea heat flux and enables the formation and persistence of sea ice during autumn and winter? A key element here is the vertical redistribution of heat (for the vertical heat redistribution, see general discussions, e.g., in *Liang et al.* [2015]).

Figure 1c shows the integral of vertical heat flux divergence (see definition in Text S1 in supporting information) over the upper 100 m ocean during April to June. This is equal to the vertical heat flux at the surface (air-sea heat flux; Figure 1b) subtracting that at 100 m depth. Negative values denote heat leaving the upper 100 m ocean. Strikingly, Figure 1c shows patterns of about −70 W/m^2 (dark blue)—indicating strong cooling of the upper 100 m—only between the SIE of each month and the SSIE (magenta curve). The associated magnitude is similar to that in Figure 1b, which suggests that for this area, there is a nearly zero vertical heat flux across 100 m depth. In a strong contrast, to the north of the SSIE, although Figure 1b shows ~ −70 W/m^2 (dark blue), Figure 1c generally shows only ~0 W/m^2 (nearly white; some local areas even show as red/positive, as explained in section 4). This indicates that vertical heat flux, as a whole, generally contributes almost zero cooling to the upper 100 m for this area, in the presence of a strong heat loss from the ocean to the atmosphere. In other words, there is a strong upward heat flux at 100 m depth that nearly balances that at the surface (the surface heat loss to the atmosphere). This heat flux is largely associated with upper ocean convection, as discussed later in this section. This is illustrated by the schematic of red arrows in Figure 3f. Scaling analysis shows that ~70 W/m^2 surface cooling flux during April to September (Figures 1b and S2b), if not compensated by convective heat flux, would trigger much more ice formation (at least 5° latitudes further north) than reality. In reality, the presence of convective heat flux and its spatial patterns strongly influence the ice distribution, which is associated with upper-ocean stratification.

Figure 1d shows the vertical-mean stratification of the upper 100 m ocean, represented by buoyancy frequency N^2 (s^{-2}, see definition, e.g., in *Vallis* [2006]). There is a narrow band (white) for an abrupt transition of stratification (transition: red to white to blue) or mixed layer depth (white in Figure 1e). The width of the band is only $\lesssim$1° in latitude for most areas. This narrow band, which is during April to June, has remarkable agreement with the location of the edge of Antarctic maximum sea ice extent (i.e., the SSIE; magenta curve in Figure 1d). Their zonal-mean difference is only $\lesssim$1°–2° in latitude. This is much smaller than the ~10–15° latitude expansion of SIE from April to September (green to magenta, Figure 1a). This result holds not only for April to June but also for July to September (Figures S2d and S2e versus Figures 1d and 1e). This result and the other results in this study, although based on the 1992–2015 mean data, are also generally true for individual years (e.g., see Figure 1f). The agreement above, as shown later, is not a coincidence, but rather reveals the following fact: the upper ocean stratification during, as early as, April to June may put a strong preconditioning/constraint for the maximum sea ice extent that is reached months later in September.

To the north of the SSIE (from the SSIE to ~55°S), the upper 100 m ocean is unstratified ($N^2 \approx 0$; blue in Figure 1 d), due to a deep ocean mixed layer (~130–170 m depths during April to June; blue in Figure 1e; Figure 3d). Therefore, the ocean heat loss to the atmosphere (Figure 1b) makes the surface ocean denser and locally

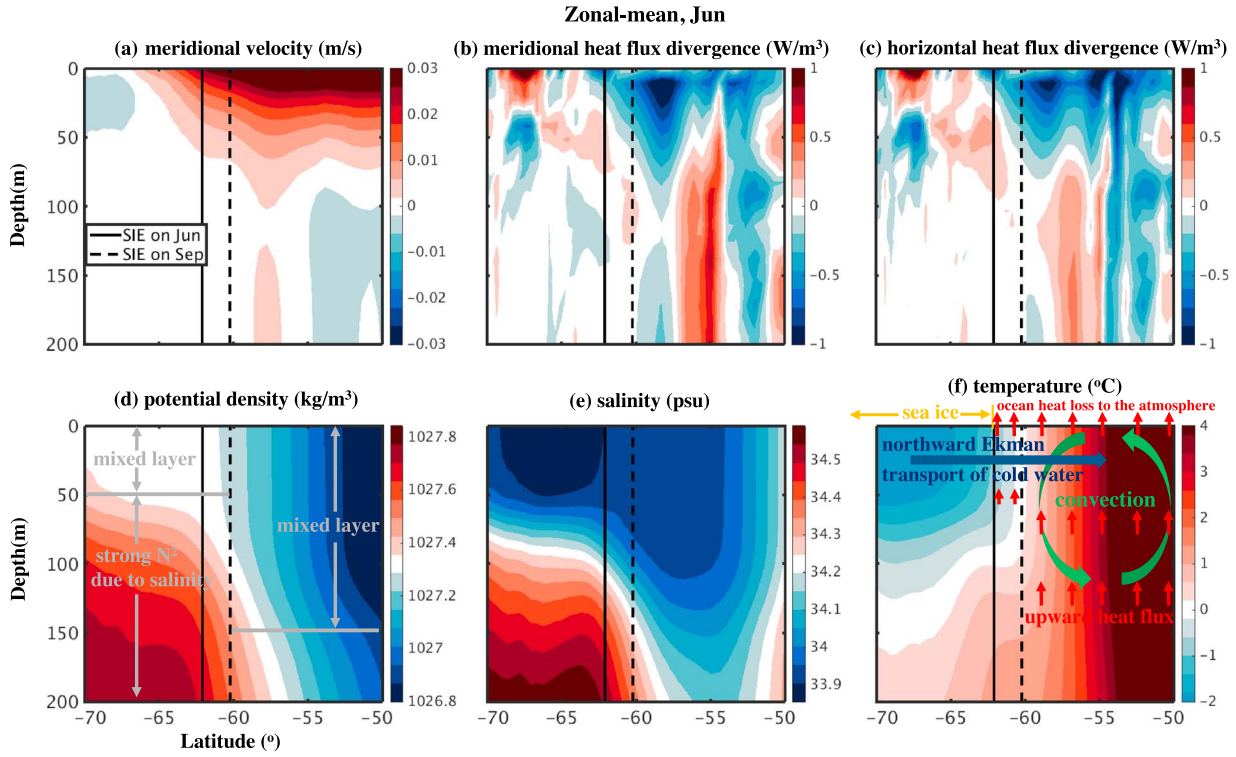

Figure 3. Zonal-mean fields in June (similar in April and May). The solid and dashed lines represent the zonal-mean latitude of sea ice edge (SIE) in June and September, respectively. (a) Meridional velocity (m/s, positive: northward). It shows significant Ekman transport in upper 100 m. (b) Meridional heat flux divergence (W/m^3, negative: to cool the ocean). The patterns in upper 100 m here are mainly caused by Ekman advection of temperature, i.e., determined by quantities shown in Figures 3a and 3f. (c) Horizontal (meridional plus zonal) heat flux divergence (W/m^3). The pattern with latitude here is consistent with Figure 2d. This is dominated by the meridional component (Figure 3c versus Figure 3b). (d) Potential density (kg/m^3) referenced to the surface pressure. The stratification is dominated by (e) salinity (psu). It induces a mixed layer depth of ~50 m (~150 m) to the south (north) of the September SIE (Figure 1e). (f) Temperature (°C) and schematics of some important processes, detailed in the text. The zonal average in all panels here is achieved along curves that parallel the September SIE rather than along constant latitudes, which makes more sense for the purpose here (these two methods lead to similar results, though).

statically unstable ($N^2 < 0$). This causes local convection: the downward motions of cold water from the surface to depths beneath 100 m (for upper ocean convection, see Skyllingstad and Denbo [1995]). This, by mass conservation, causes upward motions of relatively warm water. As a whole, convection triggers an upward heat flux in the upper ocean that nearly compensates the air-sea heat flux at the surface (white in Figure 1c, schematic by red arrows in Figure 3f). This effectively transfers the cooling effect, caused by surface heat loss to the atmosphere, from the surface downward to depths beneath 100 m (mainly to ~150 m depths). Of course, convection occurs very locally (≲0.1–10 km [see *Su et al.*, 2016a, 2016b, 2016c]) and is not resolved in ECCO v4. Its effects have been instead parameterized by vertical diffusive flux using convective mixing scheme in ECCO v4 [*Forget et al.*, 2015].

In contrast, to the south of the SSIE (from ~60°S to ~70°S), the mixed layer is much shallower during April to June (about 50–100 m; red in Figure 1e). Although rare, there exist some autumn-time observations for mixed layer depth under Antarctic sea ice. Some of these observations indicate mixed layer depths between 50 m and 100 m, which support our ECCO v4 result shown in Figure 1c (e.g., see conductivity-temperature-depth (CTD) data results in Figure 2a of *Venables et al.* [2013], Figure 3 of *Long et al.* [2012], and Figure 7c of *Wong and Riser* [2011]). There are other CTD observations that indicate mixed layer depths larger than 100 m (see Figure 1a of *Martinson and Iannuzzi* [1998]; Figures 1 and 6 of *McPhee* [2000]). The gridded data set, which combines available observations, shows that a large percentage of ocean to the South of 60°S has mixed layer depths between 50 m and 100 m in autumn [www.ifremer.fr/cerweb/deboyer/figures/mld_DReqDTm02_c1m_reg2.0.pdf; *Cabanes et al.*, 2012], which is not inconsistent with our result in Figure 1c. Overall, the related observations are still rare and very local [*Cabanes et al.*, 2012]. This unavoidably puts relatively

loose constraints on ECCO v4 state estimate for water masses below the sea ice, which is a caveat. The ocean layer between ~50 m and 100 m depth is strongly stratified (red in Figure 1d; Figure 3d) and is more statically stable than to the north, which impedes downward convective motions from crossing through. Therefore, this locks the cooling effect of air-sea heat flux vertically within the upper 100 m (dark blue in Figure 1c) and permits a cooling of this layer to the freezing point during April to September. Here using 100 m as the reference depth is deep enough, since it is overall below the mixed layer (Figure 1e) and the effect of surface heat flux is clearly trapped within the upper 100 m (Figure 1b versus Figure 1c). Once the ice cover exists, the heat loss at ocean surface is suppressed (Figure 1b). Although heat can be entrained from below [*Martinson*, 1990; *Martinson and Iannuzzi*, 1998], the base of the mixed layer is statically stable by salinity (Figure 3e) and is deepened slowly (Figure 1e), at least for ice-covered regions to the north of 70°S.

From another perspective, ocean heat loss to the atmosphere cools and deepens the mixed layer [e.g., *Marshall*, 1997]. There are two associated factors in our scenario: the mixed layer to the north of the SSIE is not only $\gtrsim$3 times deeper, but also deepened much more quickly than that to the south (Figure 1e, more dark blue with time). A much quicker deepening here is partly due to a weaker stratification beneath the mixed layer to the north than that to the south (Figure 3d; see more explanation in Text S2). These two factors both cause a much more effective mixed layer cooling (or ocean surface cooling) to the south than to the north (~ -70 versus -10 W/m^2 in terms of the upper 100 m), although both areas are under the same magnitude of air sea heat flux (~ -70 W/m^2; Figure 1b). This ~ -10 W/m^2 to the north is too weak to cool the upper ocean to the freezing point (Figure 3f) within the timescale of a few months (e.g., by scaling it costs ~30 months to cool the top 100 m from 0°C to the freezing point under -10 W/m^2, far beyond the winter timescale). So it can be neglected as an approximation, without affecting our analysis.

The stratification pattern of the upper 100 m ocean (Figures 1d and 3d), which mainly occurs at around 50–100 m depths, is caused by salinity, rather than temperature (Figures 2a and 2b and 3d–3f): they both increase with depth. This is consistent with observations (e.g., World Ocean Atlas [see Figure 1 of *Nycander et al*., 2015]). Here the salinity has a strong vertical gradient in the presence of brine rejection during the winter. This is because, to the south of SSIE, the influence of water masses around 50–100 m depths, which are about unseasonal and stratifying, is larger than the seasonal and destratifying brine rejection in determining the upper 100 m stratification. Quantitatively, the stratification is reduced by ~30% during June to September, mainly due to brine rejection, but the stratification still remains strong in September. Therefore, although the SST and air-sea heat flux are crucial factors for sea ice production, salinity (and hence salinity flux) may significantly modulate this process by dominating the stratification. Thus, freshwater fluxes can influence the upper ocean convection/entrainment and hence the ice growth, via modulating the salinity budget [e.g., *Martinson*, 1990; *Martinson and Wamser*, 1990].

4. Horizontal Heat Flux Modulated by Ekman Transport

Although vertical heat flux significantly modulates the northward expansion of sea ice to its maximum extent (section 2), this is only part of the physical picture. The upper Southern Ocean actually experiences a substantial cooling (~0.5–1°C monthly) during April to June, not only to the south of the SSIE but also to the north of it Figure 2c, reflecting the total heat flux divergence). The latter cannot be explained by the vertical heat flux divergence (Figure 1c), which is only ~ -10 W/m^2 and negligible (see section 3). It is explained, instead, by the horizontal heat flux divergence (Figure 2d), which is significant (~ -60 W/m^2, during April to June) to the north of the SSIE but negligible to the south of it (~ -10 to 10 W/m^2).

Consider the upper 100 m of the Southern Ocean to the south of ~55°S. As a whole, the horizontal heat flux divergence in this upper layer is dominated by the meridional component (Figure 3b versus Figure 3c; it is ~ -0.6 W/m^3 to the north of SSIE. After integrating over the upper 100 m, it is ~ -60 W/m^2, consistent with blue patterns in Figure 2d). The zonal component, in contrast, is found to be relatively small as a whole, although locally it can be large due to standing meanders ([*Thompson*, 2010]; see updated discussions, e.g., in *Bishop et al.* [2016]). We find that the meridional heat flux divergence in this upper ~100 m (Figure 3b) is dominated by Ekman transport rather than by eddy transport, although with a caveat that the eddy transport is mainly parameterized rather than resolved in ECCO v4 [*Gent and Mcwilliams*, 1990].

This result is generally consistent with recent studies: the lateral divergence of meridional heat flux by Ekman transport has been recognized as a strong cooling mechanism for the upper Southern Ocean [e.g., *Marshall et al.*, 2015; *Ferreira et al.*, 2015; *Purich et al.*, 2016]. The surface westerly wind prevails in most areas and causes a northward Ekman transport in the upper 100 m (red in Figure 3a). Locally speaking, this brings an inflow of relatively cold water from the south and an outflow of relatively warm water to the north. This causes a negative meridional heat flux divergence (blue in Figure 3b) that cools the upper ocean, especially to the north of the SSIE (~60°S, by zonal averaging). To the south of the SSIE (~60°S), the Ekman transport becomes much weaker and even southward (light blue in ~68°S in Figure 3a), since the surface wind can change sign in this region [*Stewart and Thompson*, 2013; *Large and Yeager*, 2009, Figure 6a]. This change of sign produces, locally, a weak *positive* meridional heat flux divergence (red in Figures 3b and 2d for this region), caused by the meridional gradient of velocity, rather than that of temperature (see related definitions in *Mahrt and Vickers* [2005]).

Now the interesting question is as follow: To the north of the maximum ice extent (i.e., the SSIE), why can the surface ocean *not* be cooled to the freezing point and hence enable the existence of sea ice, in the presence of negative *horizontal* heat flux divergence (blue in Figures 2d and 3c)? From the diagnosis of ECCO v4, we find that there are mainly two reasons. First, the inflow of relatively cold water from the south, as carried northward by the Ekman transport, mixes with local warmer water (blue versus red in Figure 3f). The resulting mixture is always warmer than the inflow of cold water due to the nature of mixing. Therefore, even though the inflow is at the freezing point, the resulting local water mixture is always warmer than the freezing point and cannot form sea ice. Second, the upper ocean Ekman inflow from the south is *denser* and colder than the local water (white versus blue in Figure 3d and blue versus red in Figure 3f). Again, the upper ocean here (to the north of SSIE), since it is unstratified (blue in Figure 1d), cannot hold parcels that are given any negative buoyancy forcing (either by air-sea heat flux or by Ekman transport). Therefore, this *denser* and colder water sinks and causes upward motion of warmer water following mass conservation. This contributes additional upward heat flux to the one caused by air-sea heat flux (section 3) in the upper ocean and leads to the red patterns to the north of SSIE in Figures 1c and S2c (the red patterns indicate a larger upward heat flux at 100 m depth than that at the surface). In other words, part of the negative horizontal heat flux divergence (dark blue in Figures 2d and S3d) is canceled out by a positive vertical heat flux divergence (red in Figures 1c and S2c). This cancelation becomes even more significant during July to September (Figure S3d versus Figure S2c). This cancelation prevents a continual large cooling for the upper ocean of this area.

5. Discussion

Our results should be treated with caution. First, the ECCO v4 solution does not resolve mesoscale eddies, which is important for ocean dynamics around the Antarctic margins [e.g., *Su et al.*, 2014]. The associated eddy effect is parameterized in ECCO v4 [*Gent and Mcwilliams*, 1990], but to what extent the parameterization can faithfully account for the eddy's effect on sea ice is still under investigation in the modeling community [e.g., *Bryan et al.*, 2014; *Liu et al.*, 2003]. ECCO v4 does not include submesoscale restratification, and the associated effect may not be neglected [*Fox-Kemper et al.*, 2011]. Second, this letter is certainly not a complete discussion on the question of "what determines the Antarctic maximum sea ice extent". This study does not trivialize other factors such as those mentioned in section 1. Third, this study suggests that Ekman transport can cool the ocean surface but does not *directly* lead to sea ice formation on a seasonal timescale. Further, we do not discuss the vertical heat flux associated with wind-driven Ekman pumping/upwelling, which in ECCO v4 is relatively small in the top 100 m when compared with the convective heat flux for 55°–70°S at a monthly timescale (April to September). However, these two factors (Ekman transport and Ekman pumping), if they have a significant trend in a timescale of years to decades, can be important for the trend of sea ice extent [e.g., *Ferreira et al.*, 2015; *Purich et al.*, 2016]. Fourth, we only discuss the effects of stratification on sea ice expansion. The latter, however, may have an important feedback on the former, e.g., by the sea ice melting flux that freshens the upper ocean [*Haumann et al.*, 2016; see also the last paragraph of our section 3]. Fifth, wind-driven sea ice drift is an important factor to drive the variability of sea ice extent such as the seasonal variability [*Holland and Kwok*, 2012; *Haumann et al.*, 2016]. At the ice edge during autumn and winter, the ice input by ice drift, which is important, may be melted quickly if the mixed layer is deep, by a similar mechanism discussed in section 3. Furthermore, the zonal asymmetry of sea ice drift and

the interaction between the drifted ice and SST may influence the spatial patterns of maximum ice extent we showed. These are worth exploring in a future study.

One more point should be noted in particular. The agreement between the location of the SSIE and the abrupt transition band of upper ocean stratification (Figure 1d, white versus magenta) is remarkable by considering the large seasonal variation of SIE (~10°–15° in latitude); however, it is far from exact. For example, the discrepancy can reach ~1°–2° in latitude, which also holds for individual years (Figure 1f). Furthermore, this agreement is zonally asymmetric: better agreement is found for 60°–300° longitude than for other longitudes (Figure 1d). Many factors not discussed in this study may cause this ~1°–2° discrepancy and the zonal asymmetry. The above point will be investigated further in the future.

This study has the following implications. First, for the evolution of Antarctic sea ice extent, upper ocean salinity flux may be an influential factor (e.g., by evaporation, precipitation, and mixed layer processes that influence freshwater flux). The salinity flux, however, is less constrained by observations than the heat flux [e.g., *Purkey and Johnson*, 2013]. More associated observations in the future, such as from satellites, Seagliders, pinniped data, and Argo floats, can be helpful to address this issue. Second, there is a possibility that the trend of stratification may have some influence on the trend of winter Antarctic sea ice extent [see also *Zhang*, 2007]. This possibility deserves future study, particularly considering possible trends in upper ocean stratification as suggested by *de Lavergne et al.* [2014]. This study suggests that the ocean condition provides a limit on the northward expansion of sea ice to the maximum, which could help explain why the trend of Antarctic ice extent is relatively smaller during the winter than summer [*Holland*, 2014].

Acknowledgments
The data set used in this study can be obtained from the ECCO project website (http://ecco2.org/llc_hires). General discussions about ocean-ice interaction with Andy Thompson, Ron Kwok, Dimitris Menemenlis, Ian Fenty, Ou Wang, and Hong Zhang are gratefully acknowledged. Two anonymous reviewers provided helpful comments. This research was carried out, in part, at the Jet Propulsion Laboratory, California Institute of Technology, under a contract with the National Aeronautics and Space Administration (NASA). Z.S. was supported by a NASA Postdoctoral Program (NPP) Fellowship.

References

Abernathey, R. P., I. Cerovecki, P. R. Holland, E. Newsom, M. Mazloff, and L. D. Talley (2016), Water-mass transformation by sea ice in the upper branch of the Southern Ocean overturning, *Nat. Geosci.*, *9*, 596–601, doi:10.1038/ngeo2749.

Armour, K. C., J. Marshall, J. R. Scott, A. Donohoe, and E. R. Newsom (2016), Southern Ocean warming delayed by circumpolar upwelling and equatorward transport, *Nat. Geosci.*, *9*, 554–549, doi:10.1038/ngeo2731.

Bintanja, R., G. Van Oldenborgh, S. Drijfhout, B. Wouters, and C. Katsman (2013), Important role for ocean warming and increased ice-shelf melt in Antarctic sea-ice expansion, *Nat. Geosci.*, *6*(5), 376–379.

Bishop, S. P., P. R. Gent, F. O. Bryan, A. F. Thompson, M. C. Long, and R. Abernathey (2016), Southern Ocean overturning compensation in an eddy-resolving climate simulation, *J. Phys. Oceanogr.*, *46*(5), 1575–1592.

Bitz, C. M., M. M. Holland, E. Hunke, and R. E. Moritz (2005), Maintenance of the sea-ice edge, *J. Clim.*, *18*, 2903–2921.

Bryan, F. O., P. R. Gent, and R. Tomas (2014), Can Southern Ocean eddy effects be parameterized in climate models?, *J. Clim.*, *27*, 411–425.

Buckley, M. W., and J. Marshall (2016), Observations, inferences, and mechanisms of the Atlantic Meridional Overturning Circulation: A review, *Rev. Geophys.*, *54*, 5–63, doi:10.1002/2015RG000493.

Cabanes, C., et al. (2012), The CORA dataset: Validation and diagnostics of ocean temperature and salinity in situ measurements, *Ocean Sci. Discuss.*, *9*, 1273–1312.

Comiso, J. C., and F. Nishio (2008), Trends in the sea ice cover using enhanced and compatible AMSR-E, SSM/I, and SMMR data, *J. Geophys. Res.*, *113*, C02S07, doi:10.1029/2007JC004257.

de Lavergne, C., C. de Lavergne, J. B. Palter, E. D. Galbraith, R. Bernardello, and I. Marinov (2014), Cessation of deep convection in the open Southern Ocean under anthropogenic climate change, *Nat. Clim. Change*, *4*, 278–282.

Fan, T., C. Deser, and D. P. Schneider (2014), Recent Antarctic sea ice trends in the context of Southern Ocean surface climate variations since 1950, *Geophys. Res. Lett.*, *41*, 2419–2426, doi:10.1002/2014GL059239.

Fenty, I., and P. Heimbach (2013), Hydrographic preconditioning for seasonal sea ice anomalies in the Labrador Sea, *J. Phys. Oceanogr.*, *43*(5), 863–883.

Ferrari, R., M. F. Jansen, J. F. Adkins, A. Burke, A. L. Stewart, and A. F. Thompson (2014), Antarctic sea ice control on ocean circulation in present and glacial climates, *Proc. Natl. Acad. Sci. U.S.A.*, *111*(24), 8753–8758.

Ferreira, D., J. Marshall, C. M. Bitz, S. Solomon, and A. Plumb (2015), Antarctic ocean and sea ice response to ozone depletion: A two-time-scale problem, *J. Clim.*, *28*(3), 1206–1226.

Forget, G., J.-M. Campin, P. Heimbach, C. Hill, R. Ponte, and C. Wunsch (2015), ECCO version 4: An integrated framework for non-linear inverse modeling and global ocean state estimation, *Geosci. Model Dev.*, *8*, 3071–3104.

Fox-Kemper, B., G. Danabasoglu, R. Ferrari, S. M. Griffies, R. W. Hallberg, M. M. Holland, M. E. Maltrud, S. Peacock, and B. L. Samuels (2011), Parameterization of mixed layer eddies. III: Implementation and impact in global ocean climate simulations, *Ocean Model.*, *39*, 61–78.

Gaspar, P., Y. Grégoris, and J. M. Lefevre (1990), A simple eddy kinetic energy model for simulations of the oceanic vertical mixing: Tests at station Papa and long-term upper ocean study site, *J. Geophys. Res.*, *95*, 16,179–16,193, doi:10.1029/JC095iC09p16179.

Gent, P. R., and J. C. Mcwilliams (1990), Isopycnal mixing in ocean circulation models, *J. Phys. Oceanogr.*, *20*(1), 150–155.

Goosse, H., and V. Zunz (2014), Decadal trends in the Antarctic sea ice extent ultimately controlled by ice-ocean feedback, *Cryosphere*, *8*, 453–470.

Gordon, A. L. (1981), Seasonality of Southern Ocean sea ice, *J. Geophys. Res.*, *86*, 4193–4197, doi:10.1029/JC086iC05p04193.

Haumann, F. A., D. Notz, and H. Schmidt (2014), Anthropogenic influence on recent circulation-driven Antarctic sea ice changes, *Geophys. Res. Lett.*, *41*, 8429–8437, doi:10.1002/2014GL061659.

Haumann, F. A., N. Gruber, M. Münnich, I. Frenger, and S. Kern (2016), Sea-ice transport driving Southern Ocean salinity and its recenttrends, *Nature*, *537*, 89–92.

Holland, P. R., and R. Kwok (2012), Wind-driven trends in Antarctic sea-ice drift, *Nat. Geosci.*, *5*(12), 872–875.

Holland, P. R. (2014), The seasonality of Antarctic sea ice trends, *Geophys. Res. Lett.*, *41*, 4230–4237, doi:10.1002/2014GL060172.

Kwok, R., J. Comiso, T. Lee, and P. Holland (2016), Linked trends in the South Pacific sea ice edge and Southern Oscillation Index, *Geophys. Res. Lett.*, *43*, 10,295–10,302, doi:10.1002/2016GL070655.
Large, W., and S. Yeager (2009), The global climatology of an interannually varying air–sea flux data set, *Clim. Dyn.*, *33*(2–3), 341–364.
Liang, X., C. Wunsch, P. Heimbach, and G. Forget (2015), Vertical redistribution of oceanic heat content, *J. Clim.*, *28*(9), 3821–3833.
Liang, X., and L. Yu (2016), Variations of the global net air–sea heat flux during the "hiatus" period (2001–10), *J. Clim.*, *29*(10), 3647–3660.
Li, X., D. M. Holland, E. P. Gerber, and C. Yoo (2014), Impacts of the north and tropical Atlantic Ocean on the Antarctic Peninsula and sea ice, *Nature*, *505*(7484), 538–542.
Liu, J., G.A. Schmidt, D. Martinson, D.H. Rind, G.L. Russell, and X. Yuan (2003), Sensitivity of sea ice to physicalparameterizations in the GISS global climate model, *J. Geophys. Res.*, *108*(C2), 3053, doi:10.1029/2001JC001167.
Long, M. C., L. N. Thomas, and R. B. Dunbar (2012), Control of phytoplankton bloom inception in the Ross Sea, Antarctica, by Ekman restratification, *Global Biogeochem. Cycles*, *26*, GB1006, doi:10.1029/2010GB003982.
Mahrt, L., and D. Vickers (2005), Boundary layer adjustment over small-scale changes of surface heat flux, *Boundary Layer Meteorol.*, *116*, 313–330.
Marshall, D. (1997), Subduction of water masses in an eddying ocean, *J. Mar. Res.*, *55*(2), 201–222.
Marshall, J., J. R. Scott, K. . C. Armour, J.-M. Campin, M. Kelley, and A. Romanou (2015), The ocean's role in the transient response of climate to abrupt greenhouse gas forcing, *Clim. Dyn.*, *44*, 2287–2299.
Martinson, D. G. (1990), Evolution of the Southern-Ocean winter mixed layer and sea ice open Ocean deep-water formation and ventilation, *J. Geophys. Res.*, *95*, 11,641–11,654.
Martinson, D. G., and C. Wamser (1990), Ice drift and momentum exchange in winter Antarctic pack ice, *J. Geophys. Res.*, *95*, 1741–1755, doi:10.1029/JC095iC02p01741.
Martinson, D. G., and R. A. Iannuzzi (1998), Antarctic Ocean-ice interaction: Implications from ocean bulk property distributions in the Weddell Gyre, in *Antarctic Research Series, Antarctic Sea Ice: Physical Processes, Interactions and Variability*, edited by M. Jeffries, pp. 243–271, Washington, D. C.
McPhee, M. G. (2000), Marginal thermobaric stability in the ice-covered upper ocean over Maud rise, *J. Phys. Oceanogr.*, *30*, 2710–2722.
Menemenlis, D., J.-M. Campin, P. Heimbach, C. Hill, T. Lee, A. Nguyen, M. Schodlok, and H. Zhang (2008), ECCO2: High resolution global ocean and sea ice data synthesis, *Mercator Ocean Q. Newsl.*, *31*, 13–21.
Nycander, J., M. Hieronymus, and F. Roquet (2015), The nonlinear equation of state of sea water and the global water mass distribution, *Geophys. Res. Lett.*, *42*, 7714–7721, doi:10.1002/2015GL065525.
Purich, A., W. Cai, M. H. England, and T. Cowan (2016), Evidence for link between modelled trends in Antarctic sea ice and underestimated westerly wind changes, *Nat. Comm.*, *7*, doi:10.1038/ncomms10409.
Purkey, S. G., and G. C. Johnson (2013), Antarctic Bottom Water warming and freshening: Contributions to sea level rise, oceanfreshwater budgets, and global heat gain, *J. Clim.*, *26*(16), 6105–6122.
Rocha, C. B., S. T. Gille, T. K. Chereskin, and D. Menemenlis (2016), Seasonality of submesoscale dynamics in the Kuroshio extension, *Geophys. Res. Lett.*, *43*, 11,304–11,311, doi:10.1002/2016GL071349.
Sallée, J., K. Speer, and S. Rintoul (2010), Zonally asymmetric response of the Southern Ocean mixed-layer depth to the Southern Annular Mode, *Nat. Geosci.*, *3*(4), 273–279.
Skyllingstad, E. D., and D. W. Denbo (1995), An ocean large-eddy simulation of Langmuir circulations and convection in the surface mixed layer, *J. Geophys. Res.*, *100*, 8501–8522.
Stammerjohn, S. E., D. G. Martinson, R. C. Smith, and R. A. Iannuzzi (2008), Sea ice in the western Antarctic Peninsula region: Spatio-temporal variability from ecological and climate change perspectives, *Deep Sea Res., Part II*, *55*(18), 2041–2058.
Stewart, A. L., and A. F. Thompson (2013), Connecting Antarctic cross-slope exchange with Southern Ocean overturning, *J. Phys. Oceanogr.*, *43*(7), 1453–1471.
Su, Z., A. L. Stewart, and A. F. Thompson (2014), An idealized model of Weddell Gyre export variability, *J. Phys. Oceanogr.*, *44*, 1671–1688.
Su, Z., Z. Su, A. Ingersoll, A. L. Stewart, and A. F. Thompson (2016a), Ocean convective available potential energy. Part I: Concept and calculation, *J. Phys. Oceanogr.*, *46*, 1081–1096.
Su, Z., A. P. Ingersoll, A. P. Ingersoll, A. L. Stewart, and A. F. Thompson (2016b), Ocean convective available potential energy. Part II: Energetics of thermobaric convection and thermobaric cabbeling, *J. Phys. Oceanogr.*, *46*, 1097–1115.
Su, Z., A. P. Ingersoll, and F. He (2016c), On the abruptness of Bølling–Allerød warming, *J. Clim.*, *29*, 4965–4975.
Thompson, A. F. (2010), Jet formation and evolution in baroclinic turbulence with simple topography, *J. Phys. Oceanogr.*, *40*(2), 257–278.
Turner, J., J. S. Hosking, T. Phillips, and G. J. Marshall (2013), Temporal and spatial evolution of the Antarctic sea ice prior to the September 2012 record maximum extent, *Geophys. Res. Lett.*, *40*, 5894–5898, doi:10.1002/2013GL058371.
Turner, J., J. S. Hosking, T. J. Bracegirdle, G. J. Marshall, and T. Phillips (2015), Recent changes in Antarctic Sea ice, *Philos. Trans. R. Soc. London, Ser. A*, *373*(2045), 20140163.
Vallis, G. K. (2006), *Atmospheric and Oceanic Fluid Dynamics: Fundamentals and Large-Scale Circulation*, Cambridge Univ. Press, Cambridge, U. K.
Venables, H. J., A. Clarke, and M. P. Meredith (2013), Wintertime controls on summer stratification and produc tivity at the western Antarctic Peninsula, *Limnol. Oceanogr.*, *58*(3), 1035–1047.
Wong, A. P. S., and S. C. Riser (2011), Profiling float observations of the upper ocean under sea ice off the Wilkes land coast of Antarctica, *J. Phys. Oceanogr.*, *41*, 1102–1115.
Worby, A. P., and J. C. Comiso (2004), Studies of the Antarctic sea ice edge and ice extent from satellite and ship observations, *Rem. Sens. Environ.*, *92*(1), 98–111.
Wunsch, C. (2016), Global ocean integrals and means, with trend implications, *Ann. Rev. Mar. Sci.*, *8*, 1–33.
Zhang, J. (2007), Increasing Antarctic sea ice under warming atmospheric and oceanic conditions, *J. Clim.*, *20*(11), 2515–2529.